JOM, Vol. 76, No. 5, 2024
https://doi.org/10.1007/s11837-024-06452-2

TECHNICAL ARTICLE

Exploration of $TiAl_3$ Phase Nucleation Mechanism in Al–5Ti–B Master Alloy

XIAOBING GENG,[1] CHENTONG ZHANG,[1,3,4] YAN LI,[1] QIANG YU,[2] MIN LIAO,[2] FUYUAN SHEN,[2] DINGHUI YU,[2] ZHIHUI LIAO,[2] YUN ZHU,[2] LIUQING HUANG,[1,3] and XUETAO LUO[1,3,5]

1.—Department of Materials Science and Engineering, College of Materials, Xiamen University, Xiamen 361005, China. 2.—Jiuding Fluorine Chemical Co., Ltd, Longyan 361000, China. 3.—Xiamen Key Laboratory of Electronic Ceramic Materials and Devices, Xiamen University, Xiamen 361005, China. 4.—e-mail: ctzhang@xmu.edu.cn. 5.—e-mail: xuetao@xmu.edu.cn

In the field of aluminum alloy processing, Al–5Ti–B master alloy stands out as the most widely used grain refiner. The morphology, distribution and quantity of the $TiAl_3$ phase in the master alloy are critical factors influencing refining effect. In this study, Al–5Ti–B master alloy was prepared by fluoride salt reaction method. The influences of feeding temperature (700–900°C) on the preparation of Al–5Ti–B master alloy were discussed in terms of microstructure characteristics, elemental yields, grain refinement effects and master alloy hardness. The results indicated that with the increasing of feeding temperature, the size of the $TiAl_3$ phase in the Al–5Ti–B master alloy was gradually decreased until it disappeared, with a gradual increasing of holes. The element recovery rates, refinement effects and master alloy hardness all trended downward. Furthermore, the nucleation mechanism of the $TiAl_3$ phase was discussed. Based on the impact of feeding temperature on the morphology of the $TiAl_3$ phase and the analysis of the diffusion movement of Ti element in the melt, coupled with thermodynamic theory, the difficulty of nucleation of the $TiAl_3$ phase at high temperatures was explained. This study is intended to provide a reference for the control of feeding temperature during the industrial production of high-quality Al–5Ti–B master alloy.

INTRODUCTION

Grain refinement is an essential method to optimize microstructure and mechanical properties of aluminum (Al) alloy. It not only improves the strength and toughness of Al alloy, but also reduces the generation of defects, such as hot cracks, shrinkage, porosity and composition segregation.[1–6] There are many approaches to refine grain, such as physical field refinement, rapid cooling refinement, mechanical-physical refinement and adding grain refining agent.[7] Among various methods, the added grain refining agent is generally regarded as one of the most economic and efficient methods. At present, the most widely used grain refining agent is Al–5Ti–B master alloy.[8] Its preparation methods include the fluoride salt reaction method, Ti-sponge route, self-propagating high-temperature synthesis method and so on.[9–13] The fluoride salt reaction method is the mainstream method due to low production cost, simple process and effective recycling of by-products.[14] Generally, the typical process of fluoride salt reaction method is as follows. First, the mixture of KBF_4 and K_2TiF_6 is added into high-temperature molten Al. Then, the fluoride salt is reacted adequately with molten Al though mechanical agitation. Finally, the refined alloy with removed by-products is cast, obtaining the Al–5Ti–B master alloy.

The refining mechanisms of Al–5Ti–B master alloy mainly include the carbide–boride particle theory, peritectic reaction theory, super-nucleation theory, duplex nucleation theory and so on.[15–17] Among these mechanisms, the duplex nucleation theory provides a

(Received October 17, 2023; accepted February 12, 2024; published online March 18, 2024)

more comprehensive explanation of the grain refinement process of Al–5Ti–B master alloy.[16,18] According to this theory, the $TiAl_3$ phase in the master alloy decomposes into titanium (Ti) and Al in the high-temperature Al melt. The Ti tends to gather around TiB_2 phase, forming a thin layer of $TiAl_3$ phase. The newly generated $TiAl_3$ phase undergoes a peritectic reaction with liquid phase to form α-Al, promoting grain nucleation. The theory illustrates that TiB_2 phase indirectly plays a nucleation role. Guzowski et al.,[19] found that the refining performance cannot be improved by individually adding a large number of TiB_2 particles into the Al melt, which emphasized the importance of the $TiAl_3$ phase in the refinement process. In addition, Wang and Fan et al.,[6,20] discovered that TiB_2 particles were surrounded by $TiAl_3$ in the refining process, forming a shell-like structure, which partially validated the duplex nucleation mechanism.

Based on the duplex nucleation theory, the size, quantity and distribution of the second phases, $TiAl_3$ and TiB_2, in the Al–5Ti–B master alloy are critical factors influencing the refining performance. The exothermic nature of the reaction between fluoride salt and Al melt has a significant impact on the nucleation of second phases.[10] Scholars conducted many studies on temperature control to achieve fine dispersion of $TiAl_3$ and TiB_2 phases, optimizing the refining performance of the master alloy. Li et al.,[21] suggested that TiB_2 particles prepared by the fluoride salt reaction method had a regular and independent shape, and the reaction temperature did not affect the microstructure of TiB_2. Liu et al.,[22] studied the relationship between the morphology of $TiAl_3$ and the reaction temperature by fluoride salt reaction method, finding that block-like $TiAl_3$ phase was more easily obtained at lower temperatures. Arnberg et al.,[23] analyzed the $TiAl_3$ phase in master alloy prepared at different temperatures, explaining that block-like $TiAl_3$ phase was easily obtained at low-temperature melt, while needle or rod-like $TiAl_3$ was obtained in high-temperature melt. Birol also studied the morphology of $TiAl_3$ phase at different reaction temperatures and found that the reaction temperature for preparing Al–5Ti–B master alloy by fluoride salt reaction method should not exceed 850°C.[24] However, previous studies did not deeply investigate the nucleation mechanism of $TiAl_3$ phase in Al–5Ti–B master alloy based on high-temperature state of master alloy obtained by quenching process.

In this study, Al–5Ti–B master alloy was prepared by fluoride salt reaction method, and the phase morphology of Al–5Ti–B master alloy in high-temperature was obtained by quenching process. The influences of feeding temperature (700–900°C) on the preparation of Al–5Ti–B master alloy were systematically discussed in terms of microstructure characteristics, elemental yields, grain refining performances and master alloy hardness. Furthermore, the mechanism of $TiAl_3$ phase nucleation was discussed.

EXPERIMENTAL

Materials and Methods

The expected product in this study is Al–5Ti–B master alloy. According to mass fraction, the appropriate amounts of pure Al (purity: > 99.8 wt.%, melting point: 660°C), K_2TiF_6 (purity: > 98.0 wt.%; melting point: 780°C) and KBF_4 (purity: > 96.0 wt.%, melting point: 530°C) were respectively weighed. The preparation process of Al–5Ti–B master alloy comprised the following steps. (1) The 2.6 kg K_2TiF_6 and 1.2 kg KBF_4 were evenly mixed and divided into two equal parts. (2) The 10 kg pure Al was respectively heated to a certain feeding temperature (700–900°C) in the well resistance furnace (specification: ZP-45). Then, the two parts of mixed fluoride salt were added into the Al melt in turn, at an interval of 5 min, for reaction (3) After adding the second part of mixed fluoride salt, the melt was stirred quickly with a carbon stick for 10 min and then stood for 5 min. (4) The by-products of fluoride salt reaction generated in the upper layer of the melt were poured out, and then the argon gas was utilized for degassing and slag removal. (5) The refined melt was poured into a metal mold surrounded by water to quench, obtaining Al–5Ti–B master alloy. (6) The prepared master alloy was cut, ground and polished sequentially. The process flow schematic diagram is shown in Fig. 1.

To evaluate the refining performance of Al–5Ti–B master alloy prepared at different feeding temperatures for pure Al, a ring mold method was used under the same solidification conditions. The experiment steps were as follows. (1) The 0.5 kg pure Al was put into the graphite crucible to heat to 730°C, and the upper oxidation skin of Al melt was removed. (2) One gram prepared Al–5Ti–B master alloy was added into the Al melt. The melt stood for 3 min after thorough stirring. (3) After standing, Al melt was poured into a ring mold with 75 mm outer diameter, 70 mm internal diameter and 25 mm height, obtaining the refined Al alloy ingot. (4) Refined Al alloy ingot was etched by aqua regia for the distinct show of Al grain boundaries.

Characterizations

The phase component of the Al–5Ti–B master alloy was detected by X-ray diffraction (XRD, specification: D8-A25) at 40 kV and 20 mA. The microstructure and constituents of second phases were observed by scanning electron microscope equipped with energy-dispersive spectroscopy (SEM-EDS, specification: SU-70) and three-dimensional digital microscope (specification: 2DVM 6). The contents of Ti and boron (B) in master alloy were analyzed by inductively coupled plasma optical emission spectrometer (ICP-OES, specification: iCAP7400). The hardness of master alloy was

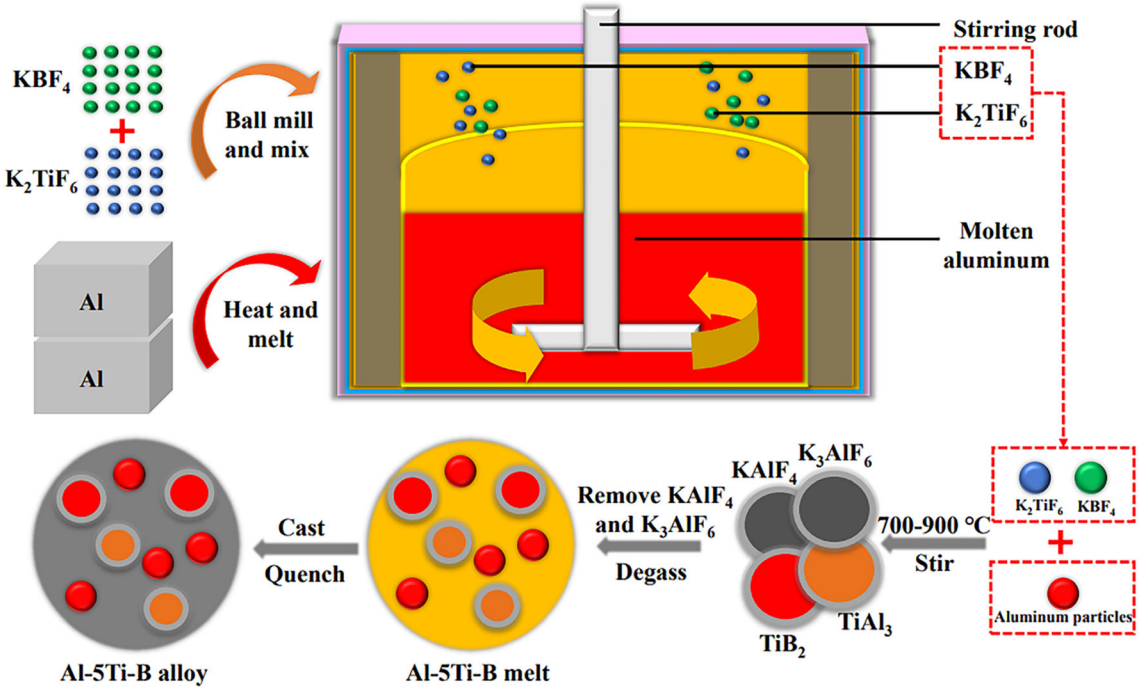

Fig. 1. Process flow of fluoride salt reaction method.

analyzed by the digital microscopic Vickers (specification: 1–1000 gf).

ANALYSIS AND RESULTS

Phase Component and Microstructure of Al–5Ti–B Master Alloy

For exploring the influence of feeding temperature on the phase component of Al–5Ti–B master alloy, XRD was employed. According to the XRD pattern shown in Fig. 2, the peaks of Al, $TiAl_3$ and TiB_2 phases were found in Al–5Ti–B master alloy obtained at 700°C feeding temperature, which indicated the product of fluoride reaction met expectations. With increasing feeding temperature, the intensity of $TiAl_3$ phase showed a gradually decreasing trend and finally almost disappeared at 900°C feeding temperature. The results indicated that the crystallization process of $TiAl_3$ phase became increasingly difficult when the feeding temperature increased from 700°C to 900°C. Concerning TiB_2 phase, its peaks were always existent with change of the feeding temperature, despite small fluctuations. Notably, there was a shift in the Al major peaks, the reason may be that the surfaces of the Al–5Ti–B master alloy samples were lower or higher than the center of the XRD optical path.[25]

The microstructure of Al–5Ti–B master alloy was observed by scanning electron microscopy and energy-dispersive spectroscopy. Figure 3a shows a representative microstructure of the Al–5Ti–B master alloy prepared at 700°C, and Fig. 3b shows a larger magnification image of a selected area in Fig. 3a. The phase boundaries of the master alloy were quite distinct;

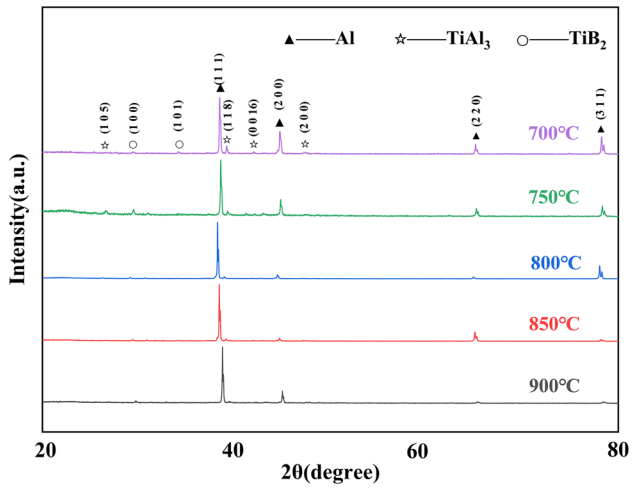

Fig. 2. XRD pattern of Al–5Ti–B master alloy prepared at various feeding temperatures.

many large gray phases and granular phases were distributed in the Al matrix. Combined with the EDS results, these phases can be respectively considered as the second phases $TiAl_3$ (Spectrum 1) and TiB_2 (Spectrum 2), which were consistent with the XRD results. The $TiAl_3$ phase presented a polygonal blocky structure. In addition, the distribution of TiB_2 phase was relatively dispersive and homogeneous, with no obvious agglomeration. In the master alloy obtained at 750°C feeding temperature, the phase boundaries were still relatively obvious, but cracks were formed on the surface of $TiAl_3$ phase, as shown in Fig. 3c. With further increasing of feeding temperature, the interior of the master alloy began to show a chaotic state. The size of $TiAl_3$ phase

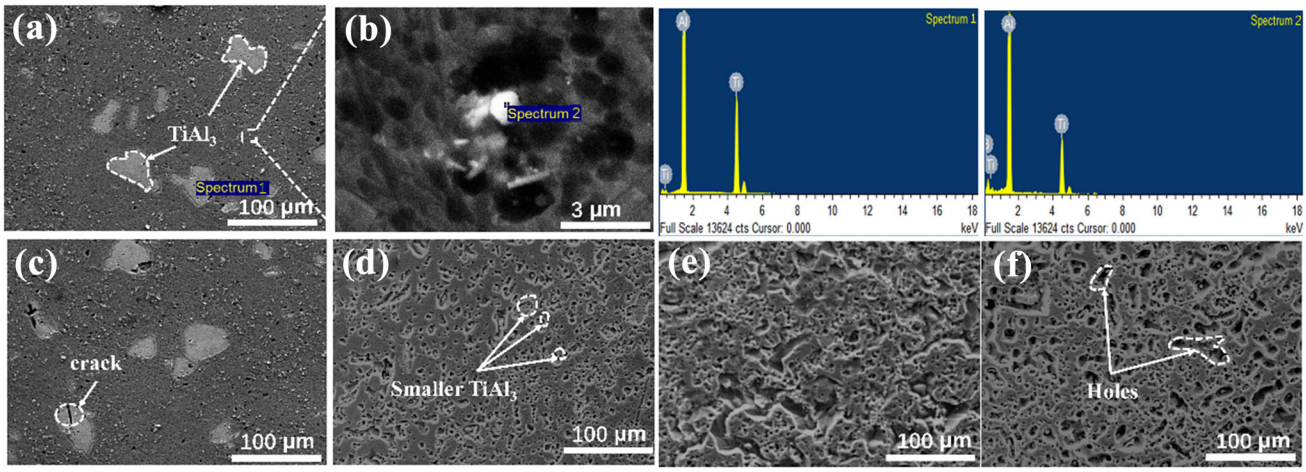

Fig. 3. Microstructure of Al–5Ti–B master alloy obtained at different feeding temperatures, (a) 700°C, (b) an enlarged region of (a), (c) 750°C, (d) 800°C, (e) 850°C, (f) 900°C and corresponding EDS analysis of second phases in master alloy.

decreased sharply, accompanied by increasing of the holes. When the feeding temperature reached 900°C, $TiAl_3$ phase disappeared basically, and holes with irregular shape and size populated the entire master alloy. The generation of the holes may be due to the different thermal expansion coefficients of Al and Ti. Ji et al.,[26] suggested that high cooling rates would lead to defects, such as considerable shrinkage and gas-type porosity. The higher the quenching melt temperature is, the faster the cooling rate, resulting in a gradual increase of holes.

For confirming the distribution of elements in the Al–5Ti–B master alloy, EDS mapping was performed, and the results are shown in Fig. 4. Ti showed strong intensity in the blocky area in the master alloy prepared at 750°C feeding temperature, which indicated that Ti was enriched obviously in the $TiAl_3$ phase. In the sample obtained at 900°C feeding temperature, although Ti gathered partially, overall it presented a dispersion state, which may be because the $TiAl_3$ phase did not grow up.

To investigate the effect of feeding temperature on the elemental yields of Al–5Ti–B master alloy, ICP-OES was applied to determine the chemical composition of the prepared samples, and the results are shown in Table I. At low feeding temperature of 700 and 750°C, the weight fractions of Ti and B were respectively close to 5% and 1%, which was consistent with the experimental expectation. However, when the feeding temperature was increased to 850 or 900°C, the fractions of Ti and B element were decreased, further deviating from pre-designed weight fractions. The reasons for this phenomenon probably included two aspects of the following. (1) When fluoride salt was added to the melt of high feeding temperature, part of it was volatilized, resulting in the loss of Ti and B. (2) According to the microstructure of Fig. 3, the Ti element in the melt cannot form $TiAl_3$ phase with Al, so some of the excess Ti and B may be stored in the upper by-product and discharged with the by-product.

Refinement Performance of Al–5Ti–B Master Alloy

The refinement performance is an important criterion to test the quality of Al–5Ti–B master alloy. The structures of solidified pure Al refined by different Al–5Ti–B master alloy and average diameters of Al grains are depicted in Fig. 5. After adding Al–5Ti–B master alloy obtained at 700°C feeding temperature, grains of pure Al were fine equiaxed grains with an average diameter of 153.8 μm. When the feeding temperature was increased, the refinement performance of Al–5Ti–B master alloy was reduced drastically, and the grain size of Al was increased markedly. The grains of pure Al refined by Al–5Ti–B master alloy obtained at 900°C feeding temperature were coarse, with an average diameter of 832.6 μm. Therefore, the influences of the feeding temperature on the refinement performance of Al–5Ti–B master alloy were remarkable. In effect, the refinement performance of Al–5Ti–B master alloy is closely related to the size, quantity and morphology of $TiAl_3$ phase.[27] According to Fig. 3, with the increase of feeding temperature, the $TiAl_3$ phase gradually disappeared, resulting in the deterioration of the refining performance of Al–5Ti–B master alloy.

Vickers Hardness Analysis of Al–5Ti–B Master Alloy

To investigate the influence of feeding temperature on the hardness of Al–5Ti–B master alloy, digital microscopic Vickers was employed. For reducing the error, ten different areas of the master alloy were respectively measured, and the average value of Vickers hardness was obtained after

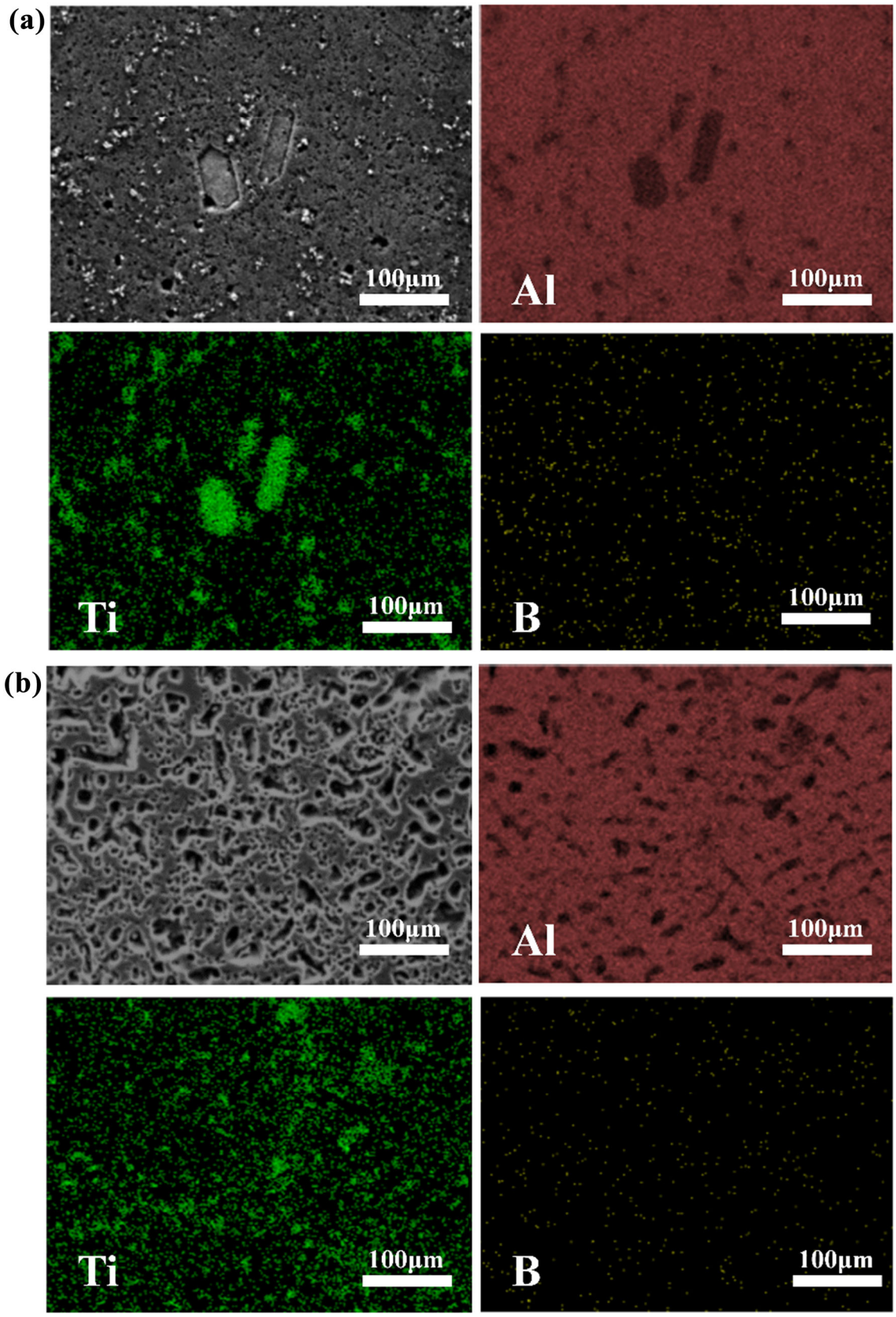

Fig. 4. EDS mapping of Al–5Ti–B master alloy prepared at different feeding temperatures, (a) 750°C and (b) 900°C.

removing the maximum and minimum values. The results are shown in Fig. 6. According to Fig. 6, the Vickers hardness of Al–5Ti–B master alloy prepared at high feeding temperature (800, 850 and 900°C) was generally lower than that prepared at low feeding temperature (700 and 750°C), which may due to the various content of $TiAl_3$ in master alloy. Thiyaneshwaran et al.,[28] investigated the influence of $TiAl_3$ content on the mechanical intensity of alloy and found that the mechanical intensity was raised with the increasing of $TiAl_3$ content.

Table I. Ti and B content in master alloy prepared at different feeding temperatures

Feeding temperature (°C)	Ti (wt.%)	B (wt.%)
700	4.98	1.03
750	5.01	1.00
800	4.95	1.02
850	4.85	0.96
900	4.82	0.90

Thermodynamic Analysis of Al–5Ti–B Master Alloy Prepared by Fluoride Salt Reaction Method

Al–5Ti–B master alloy was prepared by fluoride salt reaction method, and the main chemical reactions in the process are shown in Eqs. 1–4 as follows.[29]

$$3K_2TiF_6(s) + 13Al(l) = 3TiAl_3(s) + 3KAlF_4(s) + K_3AlF_6(s) \quad (1)$$

$$2KBF_4(s) + 3Al(l) = AlB_2(s) + 2KAlF_4(s) \quad (2)$$

$$TiAl_3(s) + AlB_2(s) = TiB_2(s) + 4Al(l) \quad (3)$$

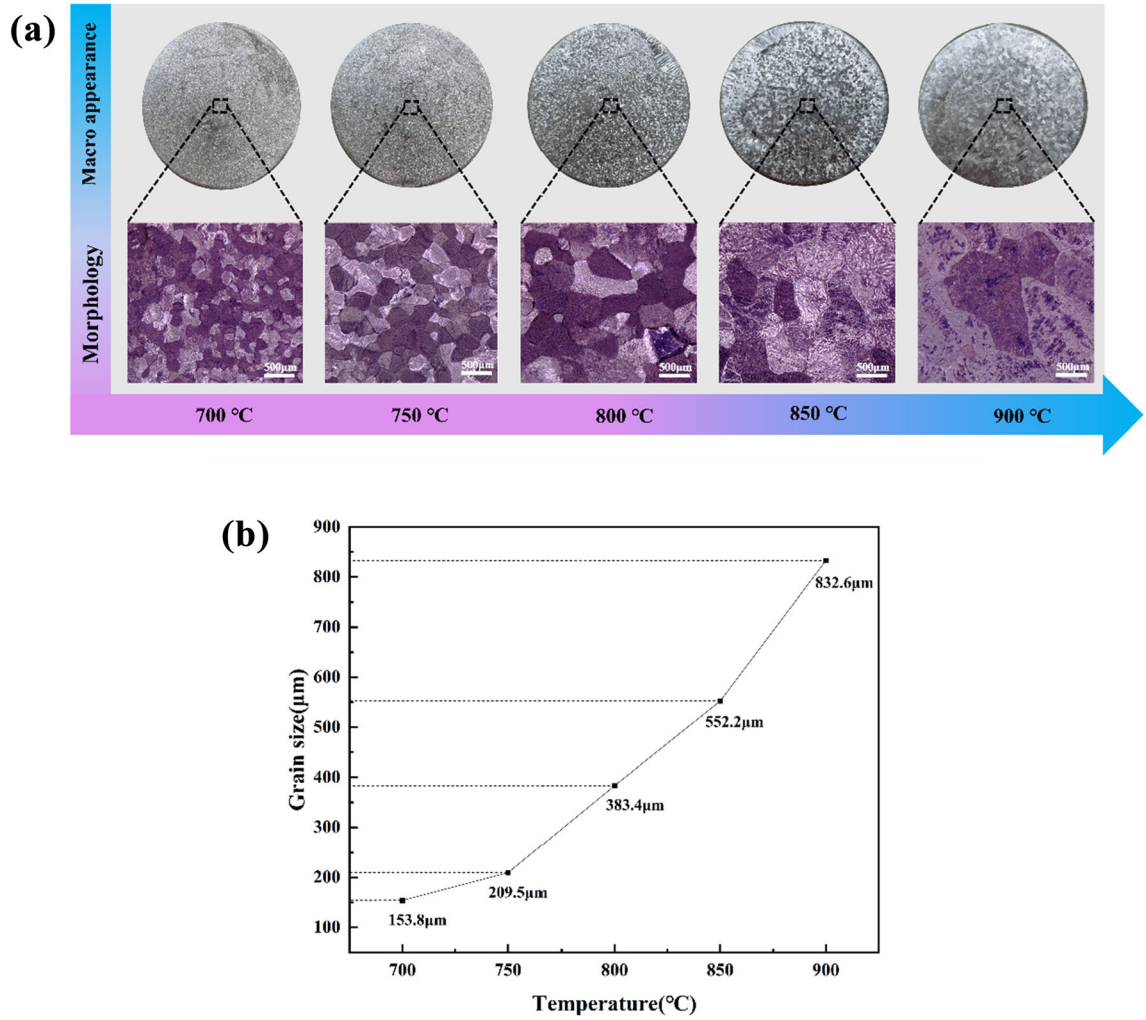

Fig. 5. (a) Macro-appearance and microstructure of pure Al refined by Al–5Ti–B master alloy prepared at different feeding temperatures and (b) influence of feeding temperature on the refinement performance of Al–5Ti–B master alloy.

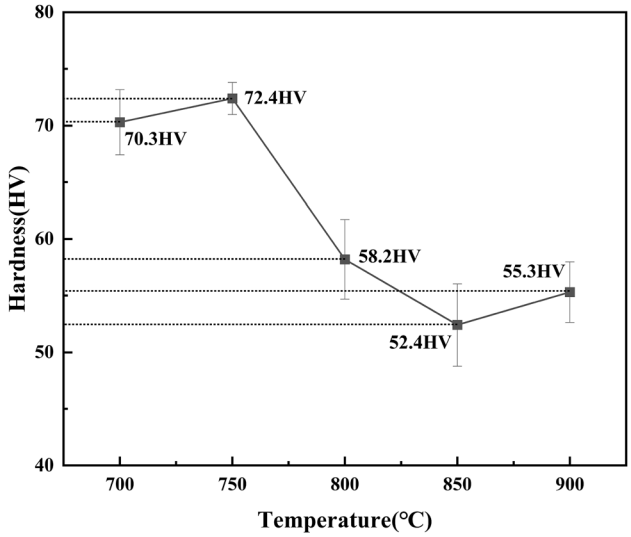

Fig. 6. Vickers hardness of Al–5Ti–B master alloy prepared at different feeding temperatures.

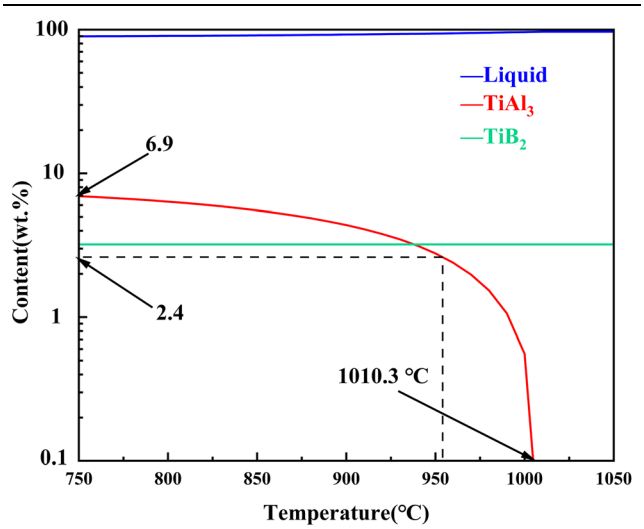

Fig. 7. Cooling process diagram of Al–5Ti–B master alloy system.

$$6KBF_4(s) + 3K_2TiF_6(s) + 10Al(l) = 3TiB_2(s) + 9KAlF_4(s) + K_3AlF_6(s) \quad (4)$$

The chemical Eq. 1 can be composed of the following two parts.

$$3K_2TiF_6(s) + 4Al(l) = 3Ti(\alpha) + 3KAlF_4(s) + K_3AlF_6(s) \quad (5)$$

$$3Al(l) + Ti(\alpha) \rightarrow TiAl_3(s) \quad (6)$$

The possible products of fluoride salt reaction contained $TiAl_3$, AlB_2, TiB_2 and slag phases such as $KAlF_4$ and K_3AlF_6.The Gibbs free energy of the formation of $TiAl_3$ and TiB_2 is shown in Eqs. 7, 8.[30] The Gibbs free energy of $TiAl_3$ was negative between 972 K (700°C) and 1172 K (900°C). As the temperature rose, its Gibbs free energy increased, which meant the generation difficulty of $TiAl_3$ phase was increased (Eq. 6). The Ti element generated by Eq. 5 was accumulated at high temperature and agglomerated in the Al–5Ti–B master alloy melt, but it was hard to form the $TiAl_3$ phase. This was consistent with the results that appeared in XRD pattern, SEM image and EDS analysis. TiB_2 is very stable, having a high melting point about 2900–3100°C.[31] Compared with $TiAl_3$, the Gibbs free energy of TiB_2 generation was lower in 700–900°C according to the Eqs. 7, 8. In melt containing Ti, Al and B elements, TiB_2 is preferentially formed. Furthermore, Emamy et al.,[32] suggested that if B was added into the Al–Ti alloy melt containing $TiAl_3$, it could form TiB_2 on the $TiAl_3$ and cause the $TiAl_3$ to break or even dissolve. In addition, Li et al.,[21] found that the morphology of TiB_2 particles in the Al–5Ti–B master alloy prepared by fluoride salt reaction method was not affected when the temperature changed from 850 to 1200°C.

$$3Al(l) + Ti(\alpha) \rightarrow TiAl_3(s) \quad \Delta G_T^{\theta} = -174389 + 55.463T\left(J\,mol^{-1}\right) \quad (7)$$

$$Ti(\alpha) + 2B(\beta) \rightarrow TiB_2(s)\Delta G_T^{\theta} = -323842 + 13.874T\left(J\,mol^{-1}\right) \quad (8)$$

Thermo-Calc Software was utilized to calculate the cooling path diagram of Al–5Ti–B master alloy system, and the result is shown in Fig. 7. Theoretically, the $TiAl_3$ phase began to nucleate at approximately 1010.3°C. With the decrease of the temperature in the Al–5Ti–B melt, the content of $TiAl_3$ phase increased. The quenching temperature of the alloy melt was measured during the process of the fluoride salt reaction, and it was found that the quenching temperature of melt reached 958°C when the feeding temperature was 900°C. According to Fig. 7, the $TiAl_3$ content in Al–5Ti–B master alloy system was about 2.4 wt.%. Due to the high quenching temperature, the $TiAl_3$ phase did not increase. The particles of $TiAl_3$ phase were small, and most of the Ti did not exist in the form of $TiAl_3$ phase. When the feeding temperature was 700°C, the quenching temperature reached 752°C, and the $TiAl_3$ content was about 6.9 wt.%. The difference in temperature had a great influence on the content of $TiAl_3$, which is consistent with the thermodynamic calculations and experimental results. As shown in Fig. 7, between 750 and 1050°C, the content of TiB_2 had no noticeable change with changing temperature.

Diffusion of Ti Element in Al–5Ti–B Master Alloy Melt

The motion of atoms in the master alloy melt was an important factor affecting the nucleation of the $TiAl_3$ phase. By studying the interfacial reaction between Ti and $TiAl_3$ at high temperature, Wu et al.,[33] found that Ti tended to diffuse to the $TiAl_3$ phase to form Ti-Al compounds of different proportions. Zhao et al.,[34] concluded that Ti-rich and B-rich regions must be formed in the melt to effectively form $TiAl_3$ and TiB_2 phases. The Ti-rich regions can be treated as the nucleation site of $TiAl_3$ phase.

To verify the existence of the Ti-rich regions, EDS linear analysis was applied to determine the distribution of Al and Ti around the $TiAl_3$ phase, the result is shown in Fig. 8. As shown in Fig. 8b, the Ti element was not uniformly distributed near $TiAl_3$ phase. Al and Ti always maintain a relatively stable ratio of 3:1 in the $TiAl_3$ phase. However, when the EDS linear analysis was performed near the outer edge of $TiAl_3$ phase, the content of Ti element was gradually reduced and finally stabilized. Schematic diagram of the diffusion of Ti element during the formation of $TiAl_3$ phase is shown in Fig. 8c. In the beginning of the nucleation, Ti was aggregated towards the nucleation site to form Ti-rich regions. When the element content of Ti was not able to meet the further growth of $TiAl_3$ phase, the excess Ti showed a slope decreasing trend around $TiAl_3$ phase. In this region, the content of Ti element maintained a proportion < 25 at.%, which was defined as Ti atomic transition zone between $TiAl_3$ phase and Al matrix in this study. The nucleation of $TiAl_3$ phase required the segregation effect of Ti element. When the content of Ti element was not enough to satisfy further growth of the $TiAl_3$ phase, the excess Ti-rich regions around $TiAl_3$ phase were transformed into the Ti transition zone.

Temperature has a certain influence on melt viscosity, and melt viscosity can affect the diffusion of elements.[35] Sun proposed that the increase of temperature would increase the interdiffusion coefficient of Ti-Al system.[36] When the temperature was low, the melt viscosity was large,[37] which hindered the diffusion of Ti to a certain extent. Ti atom can slowly deflect towards nucleation sites in the melt, it was beneficial to the accumulation of Ti element and formation of Ti-rich regions. As shown in Fig. 9a, at a lower feeding temperature (700°C), the number of Ti-rich regions was small, but the size was larger because of the influence of viscosity. The morphology of $TiAl_3$ phase was a regular block. With increasing temperature (800°C), as shown in Fig. 9b, the thermal movement of Ti element was intensified because of the decrease of melt viscosity, resulting in a decrease in the volume but an increase in the number of Ti-rich regions. The increasing number of Ti-rich regions promoted the nucleation of $TiAl_3$ phase, but the decrease of the Ti-rich regions volume inhibited the growth of $TiAl_3$ phase. As Fig. 3d shows, a smaller $TiAl_3$ phase began to appear in the alloy when the feeding temperature reached 800°C. With further

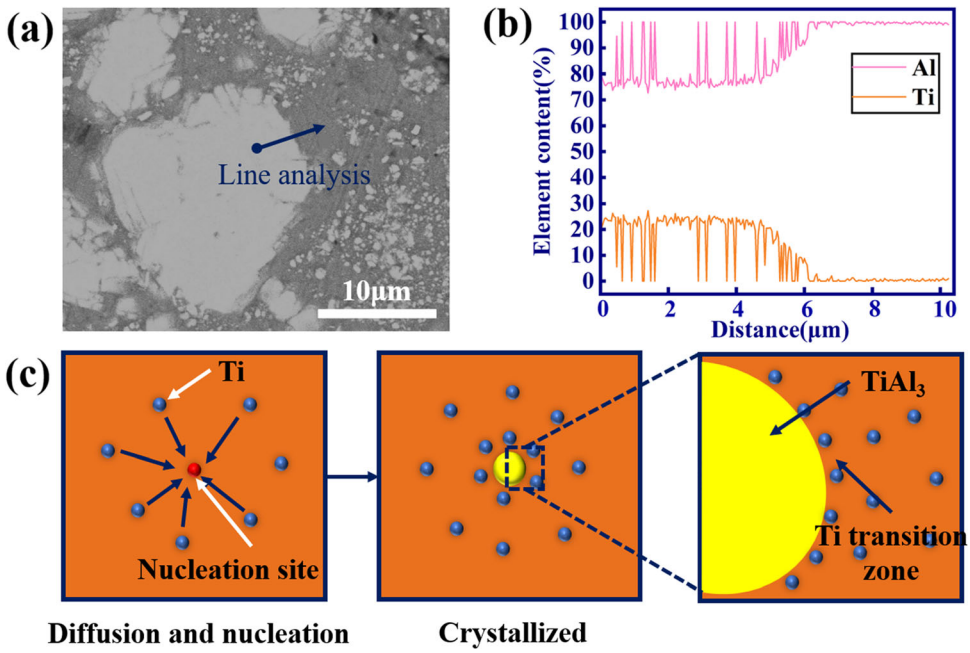

Fig. 8. (a) Microscopic view of $TiAl_3$ phase, (b) EDS linear analysis near $TiAl_3$ phase and (c) schematic diagram of the diffusion of Ti element during the formation of $TiAl_3$ phase.

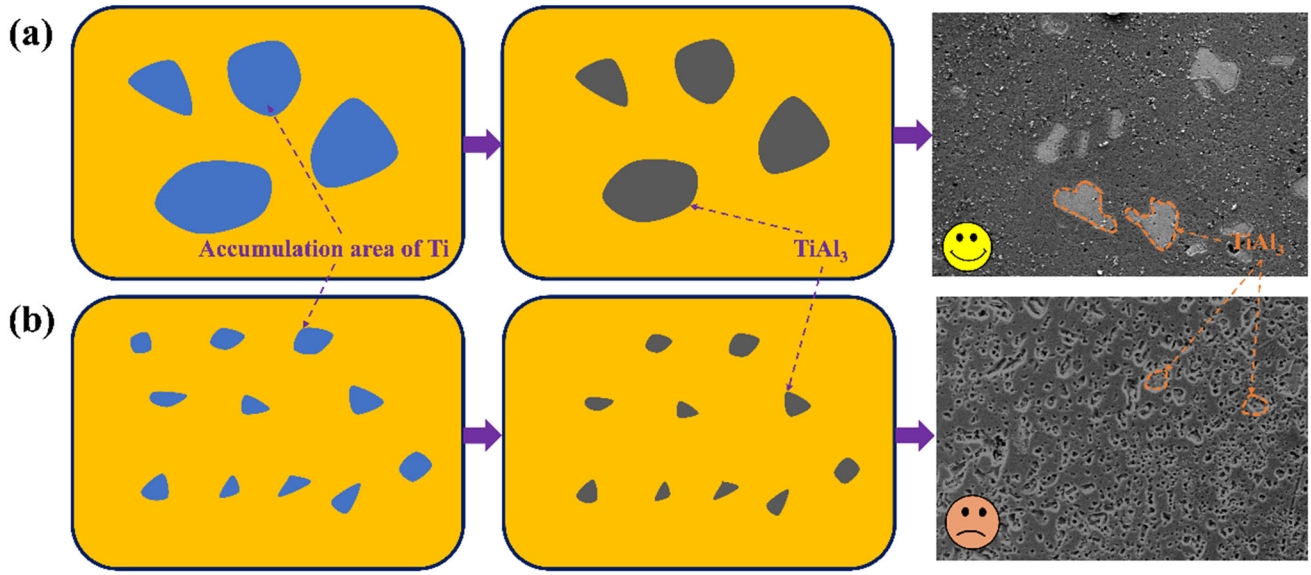

Fig. 9. Influence of feeding temperature on nucleation of $TiAl_3$ phase particles in Al–5Ti–B master alloy melt. (a) 700°C and (b) 800°C.

increasing of feeding temperature, the nucleation of $TiAl_3$ phase was thermodynamically inhibited. As TiB_2 phase preferentially consumed Ti element, the content of Ti element in melt decreased, and the volume of Ti-rich regions further decreased. Therefore, little $TiAl_3$ phase is formed at the feeding temperature of 850–900°C.

CONCLUSION

In this study, Al–5Ti–B master alloy was prepared by fluoride salt reaction method. The influences of feeding temperature (700–900°C) on the microstructure characteristics of master alloy, elemental yields, grain refinement effects and master alloy hardness were investigated, respectively. The results indicated that as the feeding temperature increased, the polygonal blocky structure of $TiAl_3$ phase in master alloy was gradually decreased until it disappeared, with the gradual increasing of holes. In addition, the elemental yields, refinement performances and master alloy hardness all showed downward trends. During the change of feeding temperature, the content and microstructure of TiB_2 maintained a relatively stable state. Furthermore, a nucleation growth mechanism of $TiAl_3$ phase was proposed based on the thermodynamics and Ti diffusion specifically as follows. The formation of Ti-rich regions was the key factor affecting the $TiAl_3$ phase nucleation. According to Gibbs free energy changes of generating $TiAl_3$ and TiB_2, the increase of feeding temperature inhibited the formation of $TiAl_3$ phase, but it did not affect the formation of TiB_2 phase. TiB_2 preferentially consumed Ti in the master alloy melt, making the remaining Ti element unable to form effective Ti-rich regions, which hindered the nucleation and growth of $TiAl_3$ phase. In addition, due to the increase of temperature, the thermal movement of Ti element in the melt was intensified, leading to the reduction of Ti-rich regions. Therefore, the nucleation of $TiAl_3$ phase was inhibited at high temperatures.

ACKNOWLEDGEMENTS

This work was supported by the industry-university-research Joint Innovation Project of Longyan City (No. 2022LYF18003) and the Technology Research and Industrial Application of New Aluminum Alloy Grain Refiner Related Products and Aphanitic Graphite Deep Purification. Thanks for the experiment conditions provided by Jiuding Fluorine Chemical Co., Ltd.

AUTHOR CONTRIBUTIONS

XG: Manuscript writing. CZ: Format modification and review. QY, ML, FS, DY, ZL, YZ: Provision and guidance of experimental equipment. YL: Thermodynamic calculations. LH: Review. XL: Project administration.

CONFLICT OF INTEREST

The authors state that they have no known competing financial interests or personal relationships that could have appeared to influence the work reported in this paper.

REFERENCES

1. J.H. Li, F.S. Hage, Q.M. Ramasse, and P. Schumacher, *Acta Mater.* 206, 116652 (2021).
2. Z. Fan, F. Gao, B. Jiang, and Z. Que, *Sci. Rep.* 10, 428 (2020).
3. Y. Li, B. Hu, B. Liu, A. Nie, and Q. Li, *Acta Mater.* 187, 51 (2020).
4. W. Ding, X. Zhao, T. Chen, H. Zhang, X. Liu, Y. Cheng, and D. Lei, *J. Alloys Compd.* 830, 154685 (2020).

5. M. Riestra, E. Ghassemali, T. Bogdanoff, and S. Seifeddine, *Mater. Sci. Eng. A* 703, 270 (2017).
6. Z. Fan, Y. Wang, Y. Zhang, T. Qin, X. Zhou, G. Thompson, T. Pennycook, and T. Hashimoto, *Acta Mater.* 84, 292 (2015).
7. J. Li, E. Wu, J. Hou, Z. Xu, H. Li, and H. Gong, *Iron Steel Vanadium Titanium China* 44, 61 (2023).
8. H. Ding, T. Zhang, Z. Zhang, and Q. Liu, *Trans. Mater Heat Treat.* 43, 31 (2022).
9. L. Zhang, H. Jiang, J. Zhao, and J. He, *J. Mater. Process. Technol.* 246, 205 (2017).
10. Y. Birol, *J. Alloy. Compd.* 443, 94 (2007).
11. H. Pourbagheri, and H. Aghajani, *Int. J. Self-Propagat. High-Temp. Synth.* 27, 245 (2018).
12. H. Li, L. Chai, H. Wang, Z. Chen, G. Shi, Z. Xiang, and T. Jin, *J. Mater.* 32, 2352 (2017).
13. S. Liu, T. Zhao, J. Fu, and Q. Zu, *Materials* 16, 3 (2023).
14. V. Auradi, and S.A. Kori, *Trans. Inndian I Metals.* 65, 637 (2014).
15. Z. Zhang, X. Bian, Y. Wang, and X. Liu, *Mater. Sci. Eng. A* 352, 8 (2003).
16. P.S. Monhanty, and J.E. Gruzleski, *Acta Metall. Mater.* 42, 2001 (1995).
17. G.P. Jones, Proceedings of International Seminar on "Refining and alloying of liquid Al and,ferro-alloys", 213 (1985).
18. K.T. Kashyap, and T. Chandrashekar, *Bull. Mater. Sci.* 24, 345 (2001).
19. M.M. Guzowski, G.K. Sigworth, and D.A. Sentner, *Metall. Mater. Trans.* 18, 603 (1987).
20. X. Wang, J. Song, W. Vian, H. Ma, and Q. Han, *Metall. Mater. Trans. B* 47, 3285 (2016).
21. P. Li, Y. Li, J. Nie, and X. Liu, *Trans. Nonferrous Met. Soc. China* 22, 564 (2012).
22. X.F. Liu, X.F. Bian, and Y. Yang, *Spec. Cast. Nonferrous Alloys* 5, 4 (1997).
23. L. Arnberg, Solidification Technology in the Foundry and Casthouse. (1980).
24. Y. Birol, *J. Alloy. Compd.* 420, 207 (2006).
25. M. Zhan, and C. Li, *Anal. Test. Technol. Instrum.* 26, 132 (2020).
26. S. Ji, Y. Wang, D. Watson, and Z. Fan, *Metall. Mater. Trans. A* 44, 3185 (2013).
27. V.M. Imayev, R.M. Imayev, and T.I. Nazarova, *Lett. Mater.* 8, 554 (2018).
28. N. Thiyaneshwaran, K. Sivaprasad, B. Ravisankar, D. Biswaranjan, and S. Karthikeyan, *J. Mater. Eng. Perform.* 31, 8483 (2022).
29. C.S. Ramesh, S. Pramod, and R. Keshavamurthy, *Mater. Sci. Eng. A* 528, 4125 (2011).
30. C. Liao, W. Chen, H. Chen, J. Fu, and C. Pan, *Chin. J. Nonferrous Met.* 26, 204 (2016).
31. X. Huang, G. Tu, S. Wang, J. Song, Y. Liu, and Z. Wang, *Rare Metal Mat. Eng.* 51, 1087 (2022).
32. M. Emamy, M. Mahta, and J. Rasizadeh, *Compos. Sci. Technol.* 66, 1063 (2006).
33. H. Wu, Y. Xu, Z. Wang, Z. Liu, Q. Li, J. Li, and J. Wu, *J. Mater. Sci. Technol.* 52, 235 (2020).
34. Y. Zhao, Z. Lu, L. Mi, Z. Hu, and W. Yang, *Materials* 15, 1984 (2022).
35. B. Xu, Y. Cao, Z. Wang, P. Du, and Y. Lon, *Minerals* 12, 925 (2022).
36. D. Sun, and L. Wang, *Shanghai Nonferrous Met.* 2, 1 (1992).
37. A. Beltyukov, V. Ladyanov, and I. Sterkhova, *J. Mol. Liq.* 296, 111764 (2019).